Lithos 286–287 (2017) 151–161

Contents lists available at ScienceDirect

Lithos

journal homepage: www.elsevier.com/locate/lithos

Iron carbide as a source of carbon for graphite and diamond formation under lithospheric mantle P-T parameters

Yuliya V. Bataleva [a,b,*], Yuri N. Palyanov [a,b], Yuri M. Borzdov [a,b], Oleg A. Bayukov [c], Evgeniy V. Zdrokov [a,b]

[a] Sobolev Institute of Geology and Mineralogy, Siberian Branch of Russian Academy of Sciences, Koptyug ave 3, Novosibirsk 630090, Russia
[b] Novosibirsk State University, Pirogova str 2, Novosibirsk 630090, Russia
[c] Kirensky Institute of Physics, Siberian Branch of Russian Academy of Sciences, Akademgorodok 50, bld. 38, Krasnoyarsk 660036, Russia

ARTICLE INFO

Article history:
Received 14 December 2016
Accepted 11 June 2017
Available online 19 June 2017

Keywords:
Iron carbide
Graphite
Diamond
Sulfur-rich fluid
Mantle sulfides
High-pressure experiment

ABSTRACT

Experimental modeling of natural carbide-involving reactions, implicated in the graphite and diamond formation and estimation of the iron carbide stability in the presence of S-bearing fluids, sulfide melts as well as mantle silicates and oxides, was performed using a multi-anvil high-pressure split-sphere apparatus. Experiments were carried out in the carbide-sulfur (Fe_3C-S), carbide-sulfur-oxide (Fe_3C-S-SiO_2-MgO) and carbide-sulfide (Fe_3C-FeS_2) systems, at pressure of 6.3 GPa, temperatures in the range of 900–1600 °C and run time of 18–40 h. During the interaction of cohenite with S-rich reduced fluid or pyrite at 900–1100 °C, extraction of carbon from carbide was realized, resulting in the formation of graphite in assemblage with pyrrhotite and cohenite. At higher temperatures complete reaction of cohenite with newly-formed sulfide melt was found to produce metal-sulfide melt with dissolved carbon ($Fe_{64}S_{27}C_9$ (1200 °C)–$Fe_{54}S_{40}C_6$ (1500 °C), at.%), which acted as a crystallization medium for graphite (1200–1600 °C) and diamond growth on seeds (1300–1600 °C). Reactions of cohenite and oxides with S-rich reduced fluid resulted in the formation of graphite in assemblage with highly ferrous orthopyroxene and pyrrhotite (900–1100 °C) or in hypersthene formation, as well as graphite crystallization and diamond growth on seeds in the Fe-S-C melt (1200–1600 °C). We show that the main processes of carbide interaction with S-rich fluid or sulfide melt are recrystallization of cohenite (900–1100 °C), extraction of carbon and iron in the sulfide melt, and graphite formation and diamond growth in the metal-sulfide melt with dissolved carbon. Our results evidence that iron carbide can act as carbon source in the processes of natural graphite and diamond formation under reduced mantle conditions. We experimentally demonstrate that cohenite in natural environments can be partially consumed in the reactions with mantle silicates and oxides, and is absolutely unstable in the presence of S-bearing reduced fluid or sulfide melt at temperatures higher than 1100 °C, under lithospheric mantle pressures.

1. Introduction

Understanding the origin and occurrences of cohenite (iron carbide, Fe_3C) is of great interest since its first documented terrestrial findings in the 1940th (Löfquist and Benedicks, 1941). Cohenite was found in native iron segregations, accompanied by abundant graphite, in basalt flows at Ovifak, Greenland. Later, very similar occurrence was revealed at Bühl, Germany (Ramdohr, 1953). At the same time in a large number of studies such occurrences of cohenite as metallic and stony meteorites were described (e.g. Brett, 1967). It was discovered, that both terrestrial and meteoritic cohenite could act as a source of metallic iron + graphite assemblage via the reaction $Fe_3C \rightarrow 3Fe^0 + C$. Reverse reaction of iron carbide formation was supposed to occur at elevated pressures, leading to a very first idea that cohenite would be a high-pressure (≥25 kbar) indicator (Ringwood, 1960). Cohenite stability under high-pressure and high-temperature conditions, characteristic of the Earth's mantle and core, is of interest since the Earth's core is probably consists not only of iron and nickel, but also of ~7 at.% of light elements, such as carbon, sulfur, oxygen etc. (Dasgupta et al., 2009; Gao et al., 2011; Wood, 1993). Cohenite is proposed to be a potential carbon-storing mineral in the inner core; however, this hypothesis is still very debatable (Dasgupta et al., 2009; Deng et al., 2013; Gao et al., 2011; Lin et al., 2004; Lord et al., 2009).

One of the main parameters affecting the cohenite stability is oxygen fugacity (fO_2). Multiple modern data, including experimental modeling results (Frost et al., 2004; McCammon, 1997; Rohrbach et al., 2007; Rohrbach and Schmidt, 2011), oxy-thermobarometry of mantle ultramafic and mafic rocks (Frost and McCammon, 2008; Stagno et al., 2011; Woodland and Koch, 2003) and theoretical analysis of the mantle fO_2 evolution (Ballhaus and Frost, 1994; Ballhaus, 1995) predicts that oxygen fugacity in the mantle rocks can be expected to decrease with increasing depth. It was experimentally demonstrated that under pressures higher than 7 GPa (≥250–300 km depth), fO_2 is low enough

* Corresponding author at: Koptyug ave 3, Novosibirsk 630090, Russia.
E-mail address: bataleva@igm.nsc.ru (Y.V. Bataleva).

http://dx.doi.org/10.1016/j.lithos.2017.06.010
0024-4937/

for the mantle to become metal-saturated, with such phases as pure metallic iron, metallic iron with dissolved carbon and iron carbides being stable (Frost et al., 2004; Frost and McCammon, 2008; Rohrbach et al., 2007; Rohrbach and Schmidt, 2011). Presence of iron carbide under these metal-saturated conditions depends on the concentration of carbon in the mantle rocks. It is shown, that at carbon content of ~30–120 ppm (depleted mantle domains) all carbon will be dissolved in metal, and at carbon content of 300–1100 ppm (undepleted mantle) it will occur as carbides (Fe_3C or Fe_7C_3), diamond and graphite (Dasgupta and Hirschmann, 2010; Frost and McCammon, 2008; Marty, 2012). Findings of cohenite as inclusions in diamonds and other mantle minerals, which are believed to have originated at different depths ranging from the upper mantle to possibly the core–mantle boundary (Jacob et al., 2004; Kaminsky and Wirth, 2011; Sharp, 1966; Smith and Kopylova, 2014; Smith et al., 2016; Torsvik et al., 2010), are undeniable evidence that iron carbide exists at great depths and participates in the global carbon cycle. Smith et al. (2016) recently showed that inclusions in large gem diamonds contain assemblages composed primarily of cohenite, Fe-Ni alloy, iron sulfide and graphite. Presence of cohenite as inclusions in diamond let us to suppose a potential genetic interconnection between these two mantle minerals and to regard iron carbide as a possible carbon source for diamond and graphite crystallization in the reduced mantle.

Several main branches among modern researches involve iron carbide studies: 1) experimental and theoretical studies on planetary evolution, core–mantle segregation, core composition (Dasgupta et al., 2009; Gao et al., 2011; Lin et al., 2004; Wood, 1993); 2) high-pressure high-temperature (HPHT) experimental works in Fe-C, Fe-Ni-C, Fe-C-S (Fe-Ni-C-S) systems (Dasgupta et al., 2009; Deng et al., 2013; Lord et al., 2009; Rohrbach et al., 2014; Tsuno and Dasgupta, 2015); 3) experimental and theoretical estimation of the stability of iron carbide in the mantle and core (Bataleva et al., 2015, 2016a; Gao et al., 2011; Rohrbach et al., 2014; Tsuno and Dasgupta, 2015); 4) studies devoted to the global carbon cycle reconstructions (e.g. Dasgupta and Hirschmann, 2010; Dasgupta, 2013; Luth, 1999). However, experimental works aimed at reconstructing the potential diamond- and graphite-forming reactions involving iron carbides are still scarce. In previous studies we have examined carbide–carbonate (Palyanov et al., 2013) and carbide–oxide (Bataleva et al., 2016a) interactions, modeling cohenite behavior in relatively oxidizing conditions, and started experimental research on the carbide–sulfur interaction (Bataleva et al., 2015). These last experimentations addressed the estimation of cohenite stability in the presence of reduced sulfur-rich fluids or melts, which are known to be mantle metasomatic agents. There we performed the very first attempt of modeling of the reactions leading to the formation of graphite and diamond from carbon extracted from cohenite via carbide–sulfur interaction. Considering the recent discovery of carbide + sulfide + metal assemblage in gem diamonds (Smith et al., 2016), which were interpreted as former Fe-Ni-C-S melt (with minor dissolved components), our results implying a participation of carbide and sulfur-rich agents can potentially shed the light on the mechanisms of diamond formation from this Fe-Ni-C-S melt under reducing conditions in the lithospheric mantle. In the present study we report new results from experimental modeling of natural carbide-involving reactions in the carbide-sulfur, carbide-sulfur-oxide and carbide-sulfide systems. These reactions are implicated in the graphite and diamond formation and allow estimation of the iron carbide stability in the presence of S-bearing fluids and sulfide melts, as well as estimation of a possibility of the transfer of iron from carbide to mantle silicates and oxides.

2. Materials and methods

Experiments were carried out using a multi-anvil high-pressure "split-sphere" apparatus (BARS) (Palyanov et al., 2010) in Fe_3C-FeS_2, Fe_3C-S, and Fe_3C-S-SiO_2-MgO systems at the pressure of 6.3 GPa, in the temperature range of 900–1600 °C, and a run duration of 18 to 40 h. Methodical features of the assembly and high pressure cell design as well as the calibration data were published previously (Pal'yanov et al., 2002; Sokol et al., 2015). As initial reagents, we used iron carbide (cohenite, Fe_3C), which was preliminarily synthesized in a Fe-C system at P = 5.7 GPa and T = 1450 °C, MgO, SiO_2, and S (<0.01 wt.% of impurities) as well as natural pyrite (<0.05 wt.% of impurities) from the Astaf'evskaya deposit (Urals, Russia). The proportions of initial materials (Table S-1) for the Fe_3C-FeS_2 and Fe_3C-S systems were selected to form a pyrrhotite + graphite assemblage upon reactions (1), (2) completion and an orthopyroxene, pyrrhotite, and elemental carbon assemblage reaction (3) in the case of a more complex Fe_3C-S-SiO_2-MgO system:

$$Fe_3C + 3S \rightarrow 3FeS + C^0 \quad (1)$$

$$Fe_3C + 3FeS_2 \rightarrow 6FeS + C^0 \quad (2)$$

$$Fe_3C + 3S + MgO + SiO_2 \rightarrow 3FeS + MgSiO_3 + C^0 \quad (3)$$

Experiments were made using a traditional design of the ampoule assembly where initial reagents were thinly ground and thoroughly mixed. However, to simulate the processes of the interaction between carbide, sulfides, sulfur, and oxides, some part of the initial carbide was not ground but was added into charge in the form of 300–400 μm crystal fragments; in this case, we intentionally created a small excess of iron carbide relatively to the other reagents of reactions (1)–(3). To assess the possibility of diamond growth, we placed cuboctahedral diamond seed crystals (size ~500 μm) into the ampoules. Furthermore, we performed two additional experiments at T = 1500 °C, which were aimed at determining the specific mechanisms of carbide–sulfur and carbide–sulfur–oxide interactions at relatively high temperatures. The assembly scheme developed for these experiments is shown in Fig. S-1. According to this scheme, large pieces (1.5–2.5 mm) of carbide crystals were mounted in the central part of the ampoule and surrounded by finely crushed sulfur (Fe_3C-S system) or a SiO_2 + MgO mixture with an underlying sulfur layer, without direct contact of sulfur with carbide (Fe_3C-S-SiO_2-MgO system). Diamond seed crystals were also placed into the reaction volume of the ampoules.

Based on our previous experience in studying of carbides, sulfides, and sulfur under mantle P and T conditions (Bataleva et al., 2015, 2016b; Palyanov et al., 2007) and data of Dasgupta et al. (2009), graphite was chosen as appropriate capsule material. In addition, graphite capsules acted as outer buffer, setting the upper limit of fO_2 values in a sample close to the CCO equilibrium during experiments (Palyanov et al., 2007). After completion of the experiments, the graphite capsule material was thoroughly analyzed (Fig. S-2) to determine the amount of iron and sulfur transferred from the reaction volume to the graphite capsule in order to make the appropriate adjustment to mass balance calculations. Transfer of both iron and sulfur to the graphite capsule was ≪1 wt.% of the sample weight for the highest-temperature and longest-duration experiments (T = 1500 °C, t = 40 h, Fig. S-2).

Given the specificity of the studied processes resulted in the formation of elemental carbon, we performed control experiments in carbide-sulfur and carbide-sulfur-oxide systems with the use of alternative capsule materials (talc ceramics and MgO) to evaluate the potential effect of the graphite capsule material on phase formation processes (Table 1). The experiments demonstrated that products of the carbide, sulfur, and oxides interaction reacted with both MgO and talc ceramics leading to a significant loss of iron in the system. Despite the fact that capsules made of these materials proved to be unsuitable for the present study, their use demonstrated the effectiveness of carbide–sulfur and

Table 1
Results of the experiments in carbide-sulfur, carbide-sulfur-oxide and carbide-sulfide systems at P = 6.3 GPa, T = 900–1600 °C and duration of 18–40 h.

Run N	T, °C	t, h	Capsule material	Final phases	Diamond growth on seeds
[Fe_3C + FeS_2] system					
CS-982	1100	20	Gr	Po, Coh, L_1, L_2, Gr	No changes
CS-983	1200	20	Gr	L_1, L_2, Gr	No changes
CS-984	1300	20	Gr	L_1, L_2, Gr	+
CS-981	1400	20	Gr	L_1, L_2, Gr	+
CS-985	1500	20	Gr	L_1, L_2, Gr	+
[Fe_3C + S] system					
SU-1623	900	18	Gr	Po, Coh, Gr	No changes
SU-1603	1000	18	Gr	Po, Coh, Gr	No changes
SU-1620	1100	20	Gr	Po, Coh, Gr	No changes
SU-1619	1200	20	Gr	L_1, L_2, Gr	No changes
SU-1599	1300	18	Gr	L_1, L_2, Gr	+
SU-1618	1400	18	Gr	L_1, L_2, Gr	+
SU-1596	1500	18	Gr	L_1, L_2, Gr	+
SU-1607	1500	40	Gr	L_1, L_2, Gr	+
SU-1602	1600	18	Gr	L_1, Gr	+
S-1593	1100	20	Ta	Po, Ol, Gr	No changes
S-1592	1200	20	Ta	Po, Ol, Gr	No changes
S-1586	1400	18	MgO	L_1, Gr	+
[Fe_3C + S + MgO + SiO_2] system					
O-1623	900	18	Gr	Po, Opx, Py, Fpc, Co, Gr	No changes
O-1603	1000	18	Gr	Po, Opx, Co, Gr	No changes
O-1620	1100	18	Gr	Po, Opx, Gr	No changes
O-1619	1200	18	Gr	L_1, Opx, Gr	No changes
O-1599	1300	18	Gr	L_1, Opx, Gr	+
O-1618	1400	18	Gr	L_1, Opx, Gr	+
O-1596	1500	18	Gr	L_1, Opx, Gr	+
O-1607	1500	40	Gr	L_1, L_2, Ol, Gr	+
O-1602	1600	18	Gr	L_1, Opx, Gr	+
O-1593	1100	20	Ta	Po, Ol, Gr	No changes
O-1592	1200	20	Ta	Po, Ol, OPx, Gr	No changes
O-1588	1400	18	MgO	L_{sulf}, Ol, Gr	+

Note: Po – pyrrhotite, Py – pyrite, Coh – cohenite, Gr – graphite, L_1 – Fe-S melt, L_2 – Fe-S-C melt;

carbide–sulfur–oxide interactions in graphite crystallization in the presence of iron carbide as the only carbon source (Fig. S-3).

The final phases and chemical composition of produced samples were determined by microprobe analysis (Camebax-micro analyzer) and energy dispersive spectroscopy (Tescan MIRA3 LMU scanning electron microscope). Analyses of sulfide, silicate, oxide, and carbide mineral phases were taken at an accelerating voltage of 20 kV, a beam current of 20 nA, a counting time of 10 s for each analytical line, and a probe electron beam diameter of 2–4 μm. The electron beam diameter was increased to 20–100 μm when studying the composition of quenched sulfide and metal-sulfide melts in the form of microdendritic aggregates. The phase relationships in samples were studied by scanning electron microscopy. These analytical studies were conducted at the Center for Collective Use of Multi-element and Isotopic Analysis of the Siberian Branch of the Russian Academy of Sciences. Mass proportions of the final phases were calculated using the mass balance method (ordinary least squares). Mössbauer spectroscopy was used to study the composition of iron-bearing phases, valence state of iron in the phases, and distribution of iron among phases and non-equivalent positions; measurements were carried out at room temperature on a MS-1104Em spectrometer with a Co^{57}(Cr) source and a powdered absorber with a thickness of 1–5 mg/cm^2. The methodology of measurements and analysis of Mössbauer spectra was described in detail in Bataleva et al. (2016a).

3. Experimental results

3.1. Experimental results in the carbide-sulfide system

The results of experiments performed in the Fe_3C-FeS_2 system are presented in Table 1 and Fig. 1. At the lowest temperature (1100 °C), the cohenite-pyrite reaction leads to the formation of a pyrrhotite and graphite assemblage, coexisting with two melts: a Fe-S melt (sulfide melt) and a Fe-S-C melt (metal-sulfide melt with dissolved carbon) (Fig. 2a–d). The compositions of resulting phases are shown in Table 2 and Fig. 3a, mass proportions of final phases are presented in Table S-2. Under these conditions, a sample lacks cohenite, while preserved single cohenite crystals exhibit signs of recrystallization in the melts (Fig. 2d). Melt quenching is accompanied by the formation of microdendritic aggregates composed of pyrrhotite (±pyrite) and metallic iron containing dissolved carbon (Fig. 2c). At the contact between initial, relatively large, cohenite grains and pyrrhotite or melts, reaction rims of graphite and graphite-pyrrhotite aggregates (thickness ~7–40 μm) occur (Fig. 2a–d). Furthermore, graphite crystals are found directly in quenched microdendritic aggregates of iron and sulfides (Fig. 2b).

At higher temperatures (≥1200 °C), the carbide-sulfide reaction leads to the formation of graphite as well as to the generation of Fe-S and Fe-S-C melts (Fig. 2e, f). All samples contain a large number of

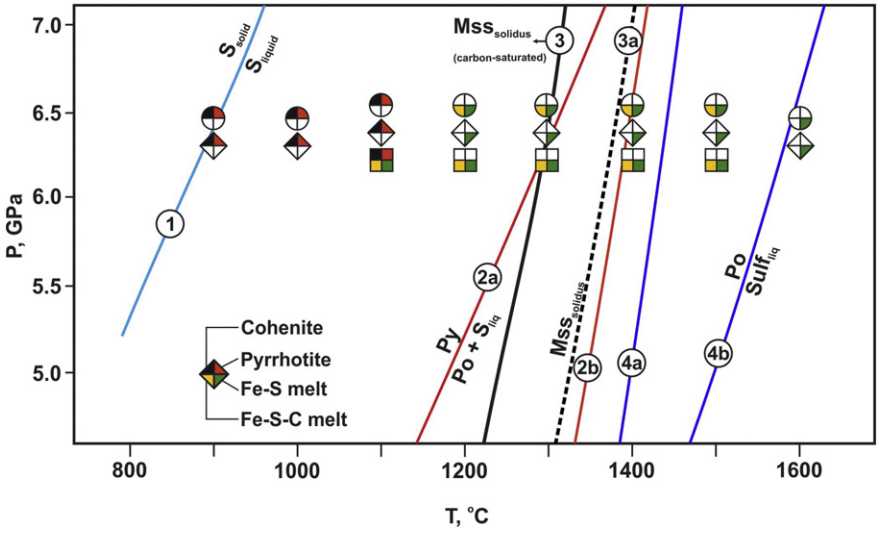

Fig. 1. Experimental results on the cohenite-sulfur (rounds), cohenite-sulfur-oxide (rhombs) and cohenite-pyrite (squares) interaction, with melting curves of S-bearing phases, experimentally determined by Brazhkin et al. (1999) (1), Sharp (1969) (2a, 2b), Zhang et al. (2015) (3), Zhang and Hirschmann (2015) and Boehler (1992) (4a, 4b). S_{liq} – sulfur melt, $Sulf_{liq}$ – sulfide melt, Po – pyrrhotite, Py – pyrite, Mss – monosulfide solid solution ($Fe_{0.69}Ni_{0.23}Cu_{0.01}S_{1.00}$).

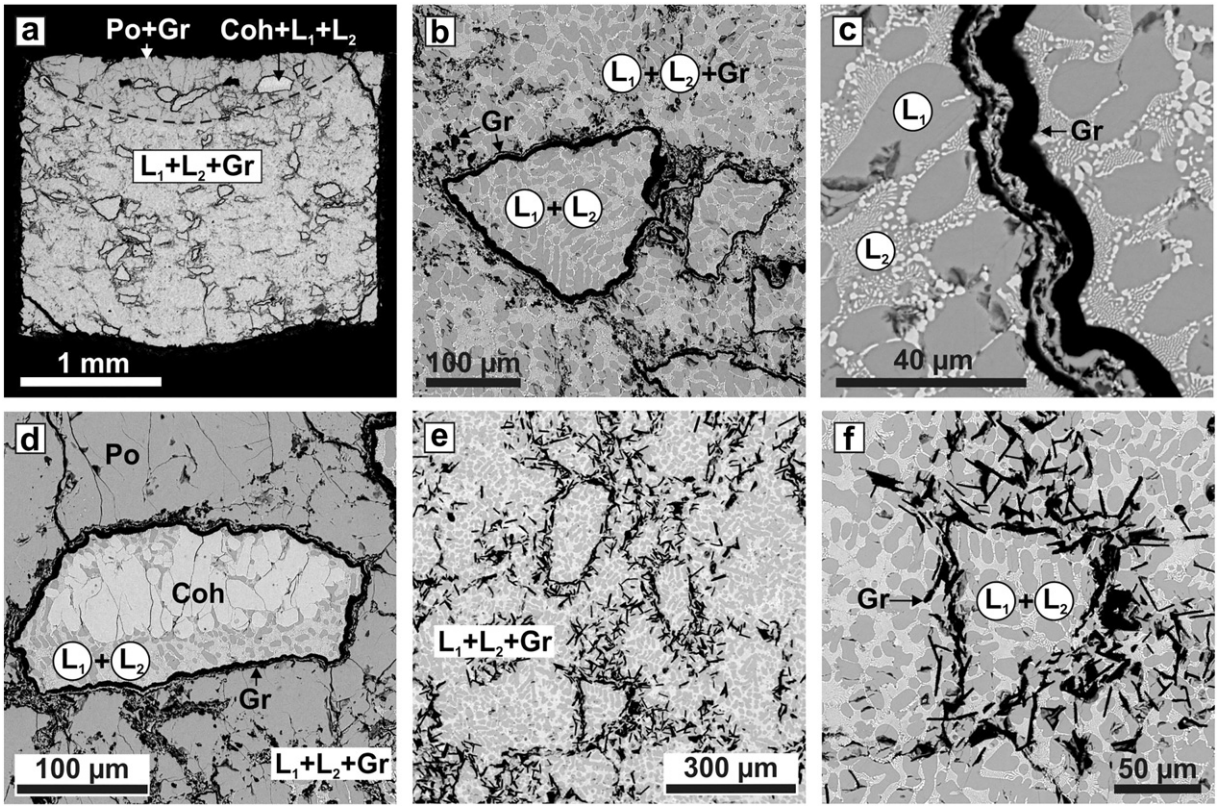

Fig. 2. SEM micro-photographs (BSE regime) of the polished sections of experimental samples (Fe_3C-FeS_2 system, T = 1100 °C (a-f) and T = 1400 °C (g–i)): a – horizontal section of the sample; b – structure of quenched melts with graphite crystals and "relict" graphite reaction rims; c – reaction rims consisted of graphite and graphite-pyrrhotite aggregates, in the quenched melts; d – quenched aggregates of Fe-S and Fe-S-C melts and recrystallized cohenite therein, edged by a graphite reaction rim; e, f – typical structure of the experimental samples at T ≥ 1200 °C; Po – pyrrhotite, Coh – cohenite, Gr – graphite, L1 - Fe-S melt, L2 - Fe-S-C melt.

graphite "relict" reaction zones delineating the border between reacted initial phases: cohenite and pyrite (Fig. 2e, f). As the experimental temperature was increased, both the structure of quenched microdendritic aggregates and the produced melt composition did not actually change (Table 2, Fig. 3a), but the features of graphite crystals are strongly temperature-dependent. In particular, the thickness of the reaction zones decreases (up to complete disappearance), while the size of the graphite plates occurring in the melt increases. At the temperatures of 1400 and 1500 °C, diamond growth is observed on the (111) and (100) faces of seed crystals (growth rate of ~6–8 μm/h).

3.2. Experimental results in the carbide-sulfur system

A detailed description of the experimental results in the carbide-sulfur system was previously published in Bataleva et al. (2015). In the present paper, we will briefly describe only the most important data. Tables 1 and 2 present the experimental results and compositions of the final phases. At the lowest temperatures (900 to 1000 °C), an assemblages of pyrrhotite ($Fe_{0.97}S$) and graphite forms, and single grains of initial cohenite are preserved. Reaction rims composed of graphite or a polycrystalline graphite-pyrrhotite aggregate are located at the border between cohenite and pyrrhotite (Fig. 4a, b). According to Mössbauer spectroscopy data (Fig. 5a; Table S-3), the newly-formed pyrrhotite is characterized by a large number of randomly distributed cation vacancies and belongs to both monoclinic (44%) and hexagonal (56%) syngonies (Table S-3). At T ≥ 1200 °C, all the samples lack carbide. In the temperature range of 1200–1400 °C, graphite crystallization is accompanied by the formation of two melts: a sulfide melt and a metal-sulfide melt with dissolved carbon. During quenching, pyrrhotite microdendrites are formed from the sulfide melt, while an aggregate of submicron iron and pyrite dendrites crystallizes from a Fe-S-C melt (Fig. 4c, d, f; Table 2). A sulfide melt produced in a temperature range of 1200–1600 °C has a constant $Fe_{0.98–0.99}S$ composition. A metal-sulfide melt containing dissolved carbon is characterized by a variable composition, with the Fe:S:C molar ratio varying from 64:27:9 (1200 °C) to 54:40:6 (1500 °C) (Fig. 3b). Mass balance calculations (Table S-2) demonstrate that the weight ratios of the produced melts are also temperature-dependent. The mass fraction of the Fe-S-C melt in the system increases from 8 wt.% (1200 °C) to 17 wt.% (1500 °C). At 1600 °C, only a quenched sulfide melt $Fe_{0.98–0.99}S$ is present in the sample (Table 2); a quenched aggregate of the melt contains large (30–40 μm) graphite crystals. It should be noted that not only graphite crystallization but also diamond growth on seed crystals (growth rate of ~5 mμ/h) occur in the melt in a temperature range of 1400–1600 °C. The results of the additional experiment (1500 °C, t = 40 h) that aimed at identifying the carbide–sulfur interaction mechanism at relatively high temperatures are shown in Fig. S-1. According to the results, the resulting samples consist primarily of quenched aggregates of a sulfide ($Fe_{0.85}S$) melt. In this aggregate, graphite crystal clusters replace initial large pieces of cohenite crystals (Fig. 4e). Diamond growth occurs on the (111) faces of seed crystals.

3.3. Experimental results in the carbide-sulfur-oxide system

At relatively low temperatures (900–1100 °C), the sulfur-carbide-oxide reaction leads to the formation of pyrrhotite, graphite and orthopyroxene (±pyrite, ±ferropericlase, ±coesite, ±cohenite) (Fig. 6a–d). As in simpler systems, graphite in samples occurs mainly in the form of reaction rims around grains of preserved cohenite (Fig. 6d). The samples also contain unusual microstructures formed by the recrystallized coesite, pyrite, and ferrosilite interaction (Fig. 6a, b). Pyrrhotite produced at T ≤ 1100 °C has a $Fe_{0.85–0.94}S$ composition (Table 2). Orthopyroxene is characterized by a variable composition:

Table 2
Averaged compositions of sulfides, carbides and melts.

Run N	T, °C	t, h	Capsule material	Phase	N_A	Mass concentrations, wt.%				Atomic concentrations, at.%		
						Fe	S	C*	Total	Fe	S	C
$Fe_3C + FeS_2$ system												
CS-982	1100	20	Gr	Po	10	63.6 (4)	37.0 (1)	–	100.6 (5)	49.5 (1)	50.5 (1)	–
				Coh	7	93.3 (0)	–	6.7 (0)	100.0	74.9 (0)	–	25.1 (0)
				L_1	12	63.5 (3)	36.7 (2)	–	100.2 (5)	49.7 (1)	50.3 (1)	–
				L_2	20	79.3 (10)	20.0 (8)	0.6 (0)	99.8 (4)	67.6 (6)	29.9 (6)	2.5 (0)
CS-983	1200	20	Gr	L_1	14	62.7 (2)	36.4 (2)	–	99.1 (1)	49.6 (1)	50.4 (1)	–
				L_2	22	78.2 (6)	20.9 (6)	0.9 (2)	100.0	65.9 (10)	30.8 (1)	3.4 (9)
CS-984	1300	20	Gr	L_1	14	62.8 (3)	36.3 (3)	–	99.1 (2)	49.7 (1)	50.3 (1)	–
				L_2	23	78.9 (2)	20.8 (3)	0.2 (0)	100.0	67.8 (2)	31.3 (2)	0.9 (0)
CS-981	1400	20	Gr	L_1	17	63.1 (4)	36.3 (3)	–	99.5 (3)	49.8 (0)	50.2 (0)	–
				L_2	22	78.6 (6)	21 (5)	0.3 (1)	100.0	67.3 (13)	31.5 (2)	1.2 (3)
CS-985	1500	20	Gr	L_1	14	64.0 (2)	36.9 (1)	–	100.9 (1)	49.8 (0)	50.2 (0)	–
				L_2	24	79.1 (7)	20.5 (9)	0.4 (1)	100.0	67.7 (9)	30.7 (6)	1.6 (4)
$Fe_3C + S$ system												
SU-1623	900	18	Gr	Po	9	62.7 (1)	36.6 (2)	–	99.3 (1)	49.5 (1)	50.5 (1)	–
				Coh	7	93.3 (1)	–	6.7 (1)	100.0	74.9 (3)	0.0	25.1 (3)
SU-1603	1000	18	Gr	Po	10	63.2 (1)	36.5 (2)	–	99.8 (2)	49.7 (1)	50.3 (1)	–
				Coh	7	93.3 (1)	–	6.7 (1)	100.0	74.9 (3)	–	25.1 (3)
SU-1620	1100	20	Gr	Po	9	63.6 (1)	36.3 (1)	–	99.9 (1)	50.0 (0)	50.0 (0)	–
SU-1619	1200	20	Gr	L_1	16	63.0 (6)	36.8 (7)	–	99.8 (6)	49.5 (3)	50.5 (3)	–
				L_2	21	78.9 (10)	18.8 (11)	2.3 (1)	100.0	64.3 (8)	26.9 (9)	8.8 (1)
SU-1599	1300	18	Gr	L_1	15	63.2 (2)	36.5 (2)	–	99.8 (1)	49.7 (1)	50.3 (1)	–
				L_2	21	75.3 (12)	22.9 (11)	1.8 (3)	100.0	60.9 (12)	32.4 (4)	6.6 (9)
SU-1618	1400	18	Gr	L_1	17	63.0 (5)	36.0 (4)	–	99.0 (5)	50.0 (1)	50.0 (1)	–
				L_2	24	71.2 (8)	27.1 (9)	1.8 (2)	100.0	56.1 (8)	37.4 (3)	6.4 (6)
SU-1596	1500	18	Gr	L_1	14	62.8 (5)	37.2 (3)	–	100.0 (4)	49.1 (2)	50.9 (2)	–
				L_2	23	68.9 (5)	29.4 (6)	1.8 (2)	100.0	53.5 (6)	39.9 (3)	6.5 (6)
SU-1607	1500	40	Gr	L_1	17	59.2 (1)	40.3 (3)	–	99.4 (5)	45.6 (1)	54.4 (1)	–
SU-1602	1600	18	Gr	L_1	16	63.7 (9)	36.2 (8)	–	99.9 (8)	50.1 (2)	49.9 (2)	–
S-1593	1100	20	Ta	Po	10	61.7 (5)	38.6 (8)	–	100.3 (6)	47.7 (3)	52.3 (3)	–
S-1592	1200	20	Ta	Po	10	60.9 (9)	38.6 (7)	–	99.5 (6)	47.4 (1)	52.6 (1)	–
S-1586	1400	18	MgO	L_1	12	63.8 (11)	36.2 (17)	–	99.9 (7)	50.2 (7)	49.8 (7)	–
$Fe_3C + S + SiO_2 + MgO$ system												
O-1623	900	18	Gr	Po	8	59.8 (3)	39.9 (1)	–	99.7 (3)	46.2 (2)	53.8 (1)	–
O-1603	1000	18	Gr	Po	8	62.2 (8)	37.3 (8)	–	99.5 (3)	48.8 (7)	51.2 (8)	–
O-1620	1100	18	Gr	Po	9	62.0 (5)	37.4 (2)	–	99.5 (4)	48.6 (4)	51.4 (1)	–
O-1619	1200	18	Gr	L_1	14	63.1 (2)	36.6 (3)	–	99.7 (2)	49.6 (1)	50.4 (1)	–
O-1599	1300	18	Gr	L_1	14	61.4 (5)	38.2 (3)	–	99.5 (4)	47.9 (3)	52.1 (2)	–
O-1618	1400	18	Gr	L_1	15	62.8 (1)	36.7 (1)	–	99.6 (2)	49.4 (1)	50.6 (1)	–
O-1596	1500	18	Gr	L_1	13	63.0 (2)	36.6 (2)	–	99.5 (3)	49.6 (1)	50.4 (1)	–
O-1607	1500	40	Gr	L_1	17	63.1 (2)	36.5 (2)	–	99.7 (3)	49.7 (1)	50.3 (1)	–
				L_2	24	78.5 (2)	20.1 (4)	1.3 (2)	100.0 (0)	65.6 (1)	29.4 (3)	5.0 (2)
O-1602	1600	18	Gr	L_1	15	62.7 (3)	36.8 (2)	–	99.5 (3)	49.3 (3)	50.7 (2)	–
O-1593	1100	20	Ta	Po	10	59.6 (2)	40.0 (2)	–	99.6 (3)	46.0 (1)	54.0 (1)	–
O-1592	1200	20	Ta	L_1	13	60.8 (1)	38.9 (1)	–	99.7 (2)	47.1 (0)	52.9 (0)	–
O-1588	1400	18	MgO	L_1	12	61.3 (2)	38.3 (2)	–	99.6 (4)	47.8 (1)	52.2 (1)	–

Po – pyrrhotite, Coh – cohenite, L_1 – sulfide melt, L_2 – metal-sulfide melt with carbon dissolved, Gr – graphite, Ta – talc ceramics, C* - calculated from a sum deficit; N_A - the number of electron probe analyses used to obtain the average compositions. The values in parentheses are one sigma errors of the means based on replicate electron microprobe analyses reported as least units cited; 79.3 $_{(10)}$ should be read as 79.3 ± 1.0 wt.%.

from ferrosilite $Fe_2Si_2O_6$ (grain size of 1–3 μm) to hypersthene $Fe_{0.6}Mg_{1.4}Si_2O_6$ (grain size of 5–15 μm) (Table 3).

At higher temperatures (T ≥ 1200 °C), the carbide-sulfur-oxide reaction results in the formation of an orthopyroxene and graphite assemblage and a sulfide melt. In this case, graphite occurs in samples mainly as 10–30 μm thick "relict" reaction rims in a temperature range of 1200–1400 °C (Fig. 6e) and as lamellar crystals, up to 70 μm in size, located directly in a quenched aggregate of the sulfide melt in a temperature range of 1500–1600 °C (Fig. 6f). At T ≥ 1300 °C, diamond growth occurs on seed crystals. The composition of orthopyroxene is within a range of $Fe_{0.09}Mg_{1.94}Si_2O_6$–$Fe_{0.18}Mg_{1.82}Si_2O_6$, while its iron content gradually decreases as temperature increases (Fig. 3c). According to Mössbauer spectroscopy data, orthopyroxene contains only divalent iron and lacks Fe^{3+} (Table S-3). The sulfide melt has a $Fe_{0.97–0.99}S$ composition that is virtually temperature-independent (Table 2). The results of the 1500 °C experiment aimed at identifying the carbide–sulfur–oxide interaction mechanism are shown in Table 1 and Fig. S-1. The resulting samples consist from primarily polycrystalline aggregates of orthopyroxene, olivine, and graphite and quenched aggregates of Fe-S and Fe-S-C melts. Initial cohenite crystals were totally replaced by quenched aggregates and graphite, their volume significantly exceeding that in the rest of the sample, surrounded by "relict" wide reaction rim of graphite. Diamond growth occurs on the (111) and (100) faces of seed crystals (growth rate of ~5 μm/h).

4. Discussion

4.1. Reconstruction of the graphite and diamond-forming processes via the interaction of iron carbide with sulfide, sulfur, and oxides

4.1.1. Cohenite–sulfur and cohenite–sulfide interactions

The processes that occur in the carbide-sulfur system are basic for carbide-sulfide and carbide-sulfur-oxide systems. The main processes occurring in the cohenite-sulfur system at relatively low temperatures

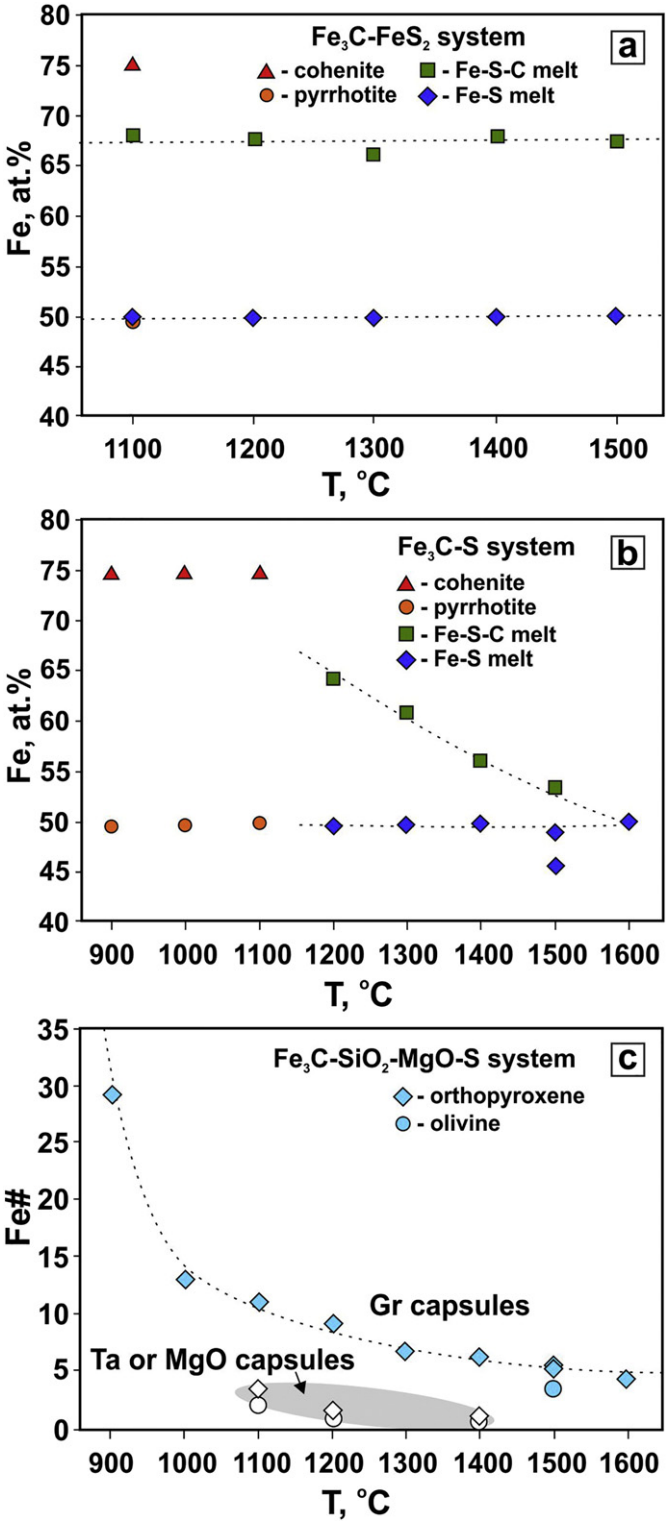

Fig. 3. Temperature dependencies of phases compositions: a, b – variations in atomic concentrations of Fe in sulfide, metal and carbide phases with temperature increase; c – decrease of Fe# (ferruginosity, Fe/(Fe + Mg) molar ratio) of orthopyroxene with temperature increase; Ta – talc.

(900–1100 °C) were found to involve melting of sulfur (Brazhkin et al., 1999) and the interaction of carbide with the melt to form a pyrrhotite and graphite assemblage according to the reaction:

$$Fe_3C_{solid} + 3S_{melt} \rightarrow 3FeS_{solid} + C^0{}_{solid} \quad (4)$$

Analysis of the reaction structures preserved around single carbide grains demonstrates that the most likely mechanism for the formation of graphite by reaction (4) is the extraction of carbon from carbide during the interaction with a sulfur melt. A distinctive feature is that pyrrhotite formed in the process belongs to the monoclinic system and has disordered vacancies, in other words, a low structural ordering degree.

At higher temperatures (T ≥ 1200 °C) in the carbide-sulfur system, melting of newly formed sulfide and crystallization of graphite occur during the interaction between cohenite and the first portions of the sulfide melt, with cohenite being completely consumed by reactions (5) and (6):

$$Fe_3C_{solid} + S_{melt} \rightarrow Fe - S_{melt} + Fe - S - C_{melt} + C^0{}_{(graphite,\ diamond\ growth)} \quad (5)$$

$$Fe_3C_{solid} + S_{melt} \rightarrow Fe - S_{melt} + C^0{}_{(graphite,\ diamond\ growth)} \quad (6)$$

As a result, part of the sulfide melt is enriched with iron and carbon resulting in the formation of a Fe-S-C melt, which subsequently serves as medium for graphite crystallization and diamond growth on seed crystals. At a temperature of 1600 °C, all carbon dissolved in the Fe-S-C melt crystallizes in the form of graphite and diamond, whereby only a Fe-S melt remains in the system.

Reconstruction of interaction processes in the carbide-sulfide system demonstrates that the main reactions occurring at the lowest temperature (1100 °C) are reactions (2) and (7):

$$Fe_3C + FeS_2 \rightarrow Fe - S_L + Fe - S - C_L + C^0 \quad (7)$$

It should be noted that reaction (2) resulting in the extraction of carbon from carbide and the formation of a pyrrhotite + graphite assemblage can occur through the interaction of carbide with both solid-phase pyrite and a sulfur melt emerging during incongruent melting of pyrite (similar to reaction (4)). However, the structure of a sample produced at 1100 °C, which consists of more than 70 vol.% quenched aggregates of Fe-S ($Fe_{0.99}S$) and Fe-S-C melts (Fig. 2a), indicates that not only decomposition of pyrite but also partial melting of newly formed pyrrhotite occurs in the system. Therefore, a temperature of 1100 °C at a pressure of 6.3 GPa is the onset temperature of partial melting of pyrrhotite under carbon-saturated conditions in a cohenite-pyrite system (bulk Fe_{47}-S_{38}-C_{15}, at.%), at which both solid-phase pyrrhotite and a $Fe_{0.99}S$ melt coexist in the system. In the sulfur-carbide system (bulk Fe_{43}-S_{43}-C_{14} at.%), the temperature of pyrrhotite partial melting onset is higher and equals to ~1200 °C. Previous experimental studies in the Fe-S system demonstrated that the solidus temperature of pyrrhotite at 6.3 GPa is of 1380 °C (Sharp, 1969) or of 1580 °C (Boehler, 1992). However, the presence of additional components in the system can lead to a significant reduction in the melting temperature. In particular, Zhang et al. (2015) demonstrated that the melting temperature of mantle sulfides in a carbon-saturated system is lower by 100–150 °C.

It is necessary to discuss the issue of the conditions for iron carbide stability in the presence of a reduced S-rich fluid/melt and sulfide melts at the mantle P-T parameters. Single cohenite grains in carbide-sulfur and carbide-sulfur-oxide systems were found to be preserved in samples at T ≤ 1100 °C. In this case, in the carbide-sulfide system at relatively low temperatures (1100 °C), cohenite is partially consumed through reaction with a sulfide melt and/or S-rich fluid; in addition, cohenite recrystallization also occurs in Fe-S and Fe-S-C melts (Fig. 2d). At higher temperatures, cohenite is completely consumed through reactions with a newly formed sulfide melt, which leads to the extraction of carbon, its crystallization in the form of graphite and diamond and to the formation of a metal-sulfide melt with dissolved carbon. These data indicate that iron carbide in the presence of S-rich

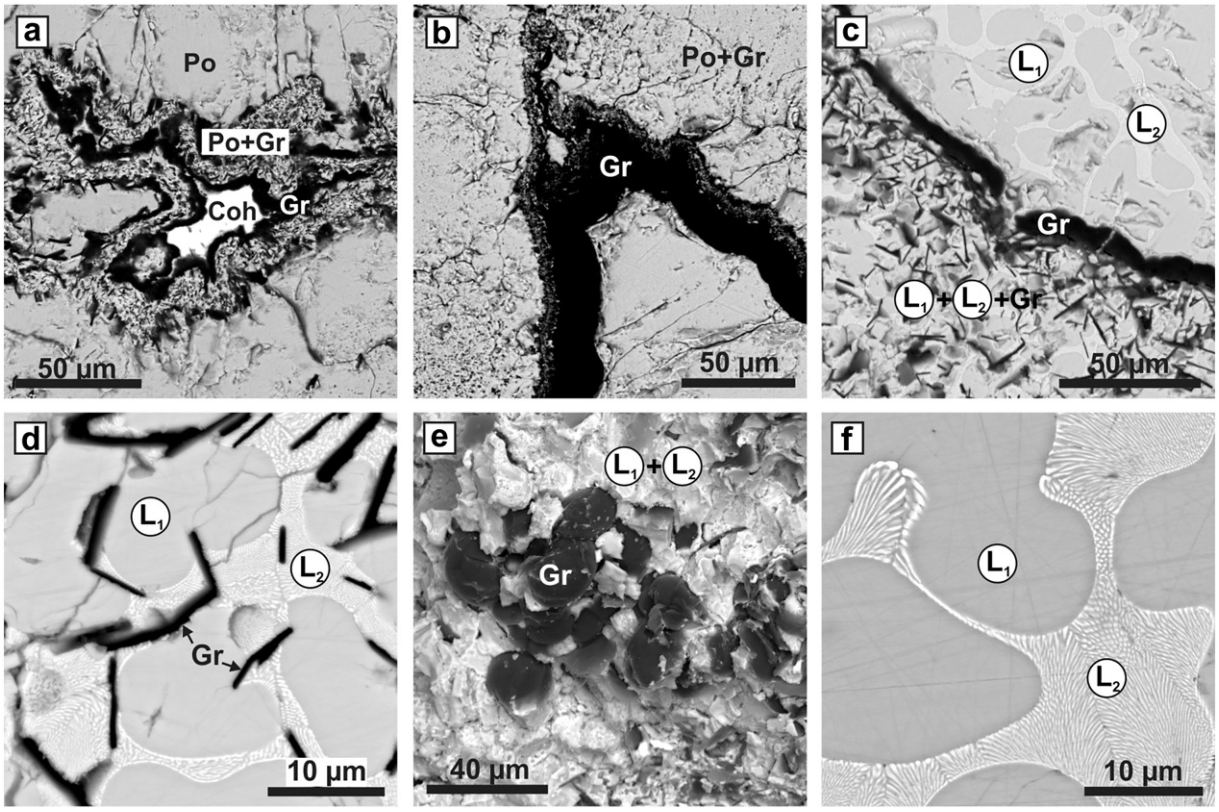

Fig. 4. SEM micro-photographs (BSE regime) of the polished sections of experimental samples (Fe_3C-S system): a – cohenite, surrounded by graphite and graphite-pyrrhotite reaction rims, in the pyrrhotite polycrystalline aggregate (900 °C); b – "relict" graphite reaction rims (1100 °C); c, d, e – graphite in the quenched aggregates of Fe-S and Fe-S-C melt (1300 °C (c, d) and 1500 °C (e)); f – structure of the quenched melts (1400 °C); Po – pyrrhotite, Coh – cohenite, Gr – graphite, L1 - Fe-S melt, L2 - Fe-S-C melt.

metasomatic agents is unstable under reduced lithospheric mantle conditions, even at relatively low temperatures (≤1100 °C).

The issue of formation of two immiscible melts of Fe-S and Fe-S-C compositions, produced by carbide–sulfur and carbide–sulfide interactions must be considered separately. Our data are in good agreement with recent experimental results (Dasgupta et al., 2009; Deng et al., 2013) obtained in Fe-S-C systems. In particular, experiments in a $Fe_{86.5}$-$S_{11.5}$-C_2 system (Deng et al., 2013) demonstrate that cohenite + pyrrhotite + Fe^0 is a stable phase assemblage at subsolidus conditions. In these studies, the composition of synthesized melts, which are in the equilibrium with graphite at 2–5 GPa and 1150–2000 °C, is in line with that of metal-sulfide melts with dissolved carbon obtained in our study. Experiments with different Fe:S:C ratios (Dasgupta et al., 2009) demonstrated that the parameters controlling immiscibility directly depend on the bulk system composition and, in particular, the amount of sulfur. For example, the immiscibility disappears at 4 GPa, 1420 °C, and 5 wt.% of sulfur and at pressure higher than 5 GPa, T ≥ 1150 °C, and 15 wt.% of sulfur. Our findings extend the understanding of phase formation in the Fe-S-C system at sulfur concentrations much higher than those in previous studies and indicate that in the system with a bulk sulfur content of 30 to 35 wt.% and pressure of 6.3 GPa, a single melt forms at T > 1500 °C.

4.1.2. Cohenite-sulfur-oxide reactions

As it was mentioned above, experiments, performed in the carbide-sulfur-oxide system, are complementary to primary carbide-sulfur and carbide-sulfide series. According to the goal of the present study, when reconstructing the interaction processes we should emphasize a question on the features of the formation of ferrous silicates or oxides cohenite-oxide reactions in the presence of S-rich reduced fluid. In other words, how can iron from carbide move into silicates as FeO through cohenite-sulfur-oxide reactions?

At relatively low temperatures (900–1000 °C), several processes occur simultaneously in the carbide-sulfur-oxide system. They include the formation of graphite and pyrrhotite (through reaction (4)), crystallization of an orthopyroxene (hypersthene), ferropericlase and pyrite assemblage, recrystallization of coesite and formation of ferrosilite. Crystallization of hypersthene, ferropericlase, and pyrite most likely occurs during the interaction of initial MgO and SiO_2 with newly formed pyrrhotite through the reaction:

$$3MgO + 2SiO_2 + 2FeS + 1/2O_2 \rightarrow (Mg,\ Fe)_2Si_2O_6 + FeS_2 + 2(Mg,Fe)O \quad (8)$$

Orthopyroxene crystallization can also occur during the interaction between initial oxides and cohenite:

$$3MgO + 4SiO_2 + 1/3Fe_3C + 1/2O_2 \rightarrow 2(Mg,Fe)_2Si_2O_6 + 1/3C^0 \quad (9)$$

Thus, it is found that in a temperature range of 900–1000 °C, iron from carbide or sulfide can be incorporated as FeO to silicate and oxide mantle phases, as a result of redox reactions (8) and (9). To scale down this incorporation to natural conditions, we should note that in the natural mantle environments carbides and sulfides, as well as S-rich fluid, occur in micro volume interstitials of rocks, with mantle silicates and/or oxides being prevailing phases. As far as we simulate carbide-involving reactions and do not investigate model systems, our results can be used only as a qualitative evidence of cohenite-silicate and cohenite-oxide iron transfer.

Special attention should be paid to the formation of coesite-pyrite-ferrosilite reactive microstructures (Fig. 6a, b) realized in samples at 900–1000 °C. These microstructures may be characterized as submicron

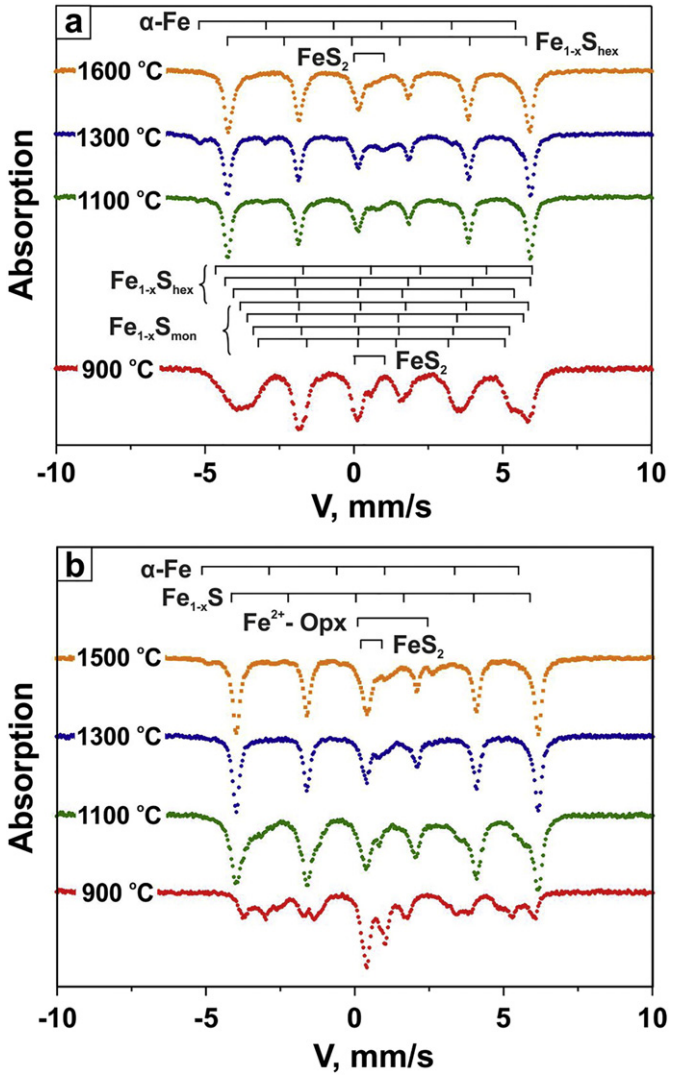

Fig. 5. Room-temperature Mössbauer spectra of representative samples from the Fe_3C-S system (a) and Fe_3C-SiO_2-MgO-S system (b); Opx – orthopyroxene.

pyrite and ferrosilite inclusions regularly distributed in recrystallized coesite. Most likely, these microstructures formed during reaction between coesite and pyrrhotite, leading to the formation of ferrosilite and pyrite:

$$2SiO_2 + 4FeS + O_2 \rightarrow Fe_2Si_2O_6 + 2FeS_2 \quad (10)$$

Further interaction of pyrite and ferrosilite with cohenite and MgO, which occurs at higher temperatures, leads to the formation of a fine-crystalline aggregate of orthopyroxene (bronzite-hypersthene), magnesiowustite, pyrrhotite, graphite, and recrystallized coesite (Fig. 6c):

$$Fe_2Si_2O_6 + FeS_2 + 1/3Fe_3C + MgO \rightarrow (Mg,Fe)_2Si_2O_6 + 2FeS + (Mg,Fe)O + 1/3C^0 \quad (11)$$

All reactions occurring in the system at 900 and 1000 °C (reactions (4), (8)–(11)) most likely occur also at T ≥ 1100 °C. However, starting from 1100 °C, only orthopyroxene, graphite, and pyrrhotite (or a quenched aggregate with the composition corresponding to that of pyrrhotite) are found in the final samples. Taking into consideration the results of the additional experiment at 1500 °C, where both Fe-S and Fe-S-C melts were registered, we suggest that during the main series of experiments on cohenite–sulfur–oxide interaction at T ≥ 1100 °C Fe-S-C melt was also formed. Consumption of cohenite during the formation of ferrous orthopyroxene and intense processes of graphite crystallization and diamond growth on seed crystals resulted in the decrease of carbon concentration in the Fe-S-C melt until, finally, only Fe-S melt remained in the system.

4.2. Implications of interaction processes of carbide with S-rich fluid and sulfide melts in natural deep mantle environments

It is accepted, that cohenite can occur in the reduced mantle environments with oxygen fugacity values close to or below those of IW (iron-wustite) buffer equilibrium, and with bulk carbon content higher than ~300 ppm (Dasgupta and Hirschmann, 2010; Frost and McCammon, 2008; Marty, 2012; Rohrbach et al., 2007; Rohrbach and Schmidt, 2011). Cohenite is also supposed to be formed in mantle domains affected by redox freezing, in other words where a carbonate, transported at great depth by subduction, interacts through redox reactions with the metal-bearing mantle (Palyanov et al., 2013; Rohrbach and Schmidt, 2011). Iron carbide stability under these conditions is controlled by the possible reactions with fO_2-contrasting minerals, introduced with subduction of oxidized crustal material (Bataleva et al., 2016a; Palyanov et al., 2013), as well as interactions with various melts and fluids – agents of mantle metasomatism. Some of the most common of those metasomatic agents are sulfur-bearing fluids and melts (either reducing or oxidizing), more specifically C-O-H-S fluids, sulfide melts or silicate melts with dissolved sulfur (e.g. Alard et al., 2011; Delpech et al., 2012; Evans, 2012; Evans and Powell, 2015).

As it was shown by Eggler and Lorand (1993), in the redox conditions characteristic for subcratonic mantle peridotites, sulfur-bearing fluids are supposed to be of H_2S composition (reduced) rather than SO_2 (oxidized), which confirms the possibility of interaction between deep mantle rocks, particularly cohenite-bearing ones, and slab-derived fluids containing reduced sulfur. Although down-going slab is the most probable source of sulfur as well as fluids and melts, by which sulfur can be mobilized, proposed mechanism of graphite and diamond crystallization can be applied to other mantle settings. Particularly, mantle plumes (Schissel and Smail, 2001) and various processes at the Earth's core-lower mantle boundary, resulting in partial melting events (Griffin et al., 2004; Haggerty, 1986; Wood et al., 2014) can be proposed as sources of melts or fluids, bearing sulfur in reduced form. In this case, the implementation area of the suggested mechanism is not limited to the subduction settings, but only by the cohenite stability field.

Our results can also be discussed in terms of their possible implications to the problem of the formation of large diamonds from metallic liquid in Earth's deep mantle involving participation of subducted carbon (Smith et al., 2016). As it was shown, Fe-Ni-C-S melt (similar to the one generated in our experiments) can be both a potential source and medium for diamond crystallization in the reduced conditions prevailing in the lithospheric mantle. According to the proposed model, formation of predominantly metal melt with dissolved carbon and sulfur can occur in subducted eclogite by disproportionation, with further diamond crystallization, proceeding within pockets of this metal melt. We have established above that a Fe-S-C melt can result of interaction of iron carbide with sulfur-rich fluid or sulfide melt under metal-saturated conditions in the lithospheric mantle. Despite the differences in the melt generation processes, we believe that the mechanism of diamond formation from Fe-S-C melt reconstructed in our work complements the one proposed by Smith coauthors.

When comparing the compositions of the final phases as well as the phase associations in the obtained samples with the inclusions in natural P-type and E-type diamonds, key similarities and differences can be established. As shown above, pyrrhotite, graphite, orthopyroxene, cohenite (±coesite, pyrite, ferropericlase) were obtained as the main phases at relatively low temperatures in the Fe_3C-S-SiO_2-MgO system. All these phases were previously found both in mono- and polyphase inclusions in diamond. Most of them are characteristic for diamonds of

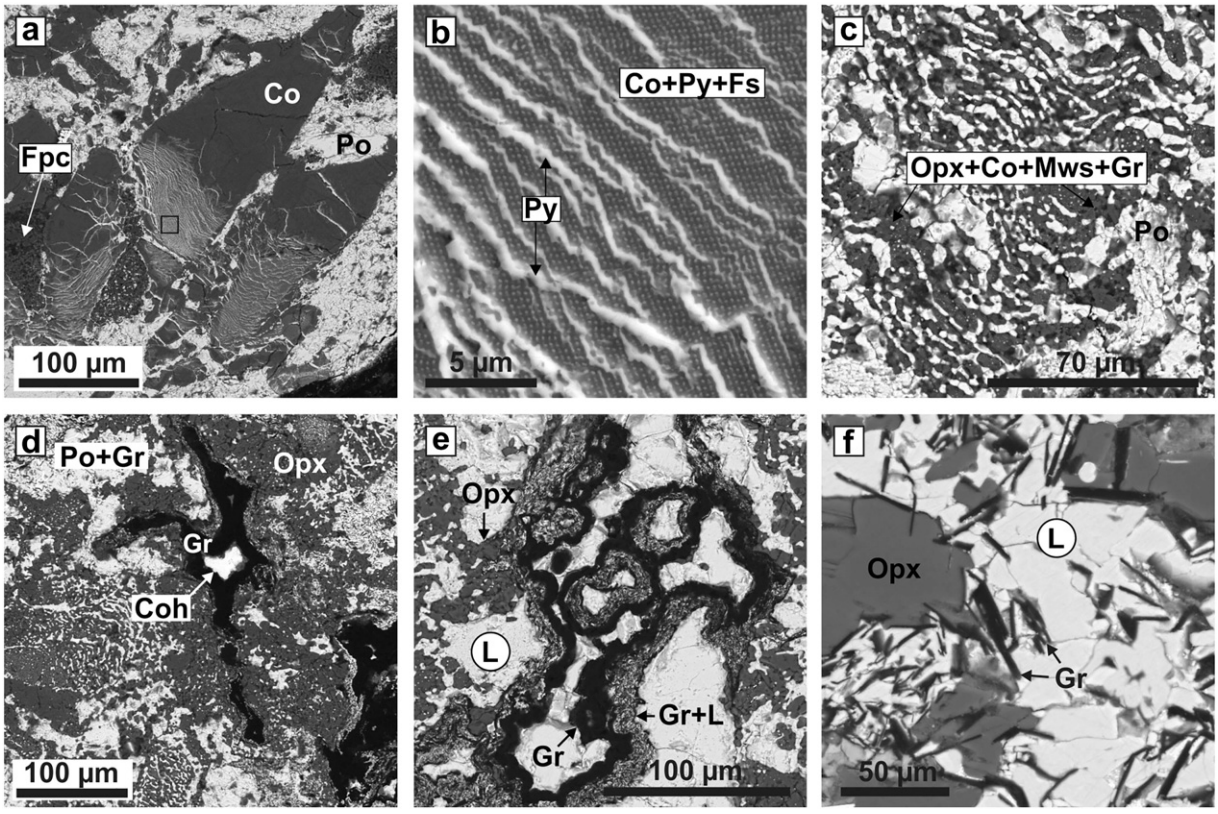

Fig. 6. SEM micro-photographs (BSE regime) of the polished sections of experimental samples (Fe_3C-SiO_2-MgO-S system): a – recrystallized coesite in the pyrrhotite-ferropericlase polycrystalline aggregate (900 °C); b – enlarged fragment of Fig. 6a, illustrating micropatterns of pyrite-coesite interaction, resulting in ferrosilite formation (900 °C); c – polycrystalline aggregate of pyrrhotite, orthopyroxene and coesite (1100 °C); d – cohenite, surrounded by a graphite reaction rim, in an orthopyroxene + pyrrhotite + graphite polycrystalline aggregate 1100 °C; e – "relict" graphite reaction rims in the quenched melt (1300 °C); f – crystals of orthopyroxene and graphite in the quenched Fe-S melt (1600 °C); Po – pyrrhotite, Co – coesite, Fpc – ferropericlase, Fs – ferrosilite, Opx – orthopyroxene, Coh – cohenite, Gr – graphite, L - Fe-S melt.

eclogite paragenesis, in particular Fe-sulfides (pyrrhotite or pyrite + pyrrhotite), graphite, cohenite, coesite, wustite and ferropericlase (e.g. Bulanova, 1995; Sobolev, 1974; Sobolev et al., 2004), and only orthopyroxene is more characteristic for inclusions in diamonds of peridotite paragenesis (Sobolev, 1974). However, it is necessary to keep in mind the fact that the proportions of the initial substances in the system were set in such a way that when the reactions were completely realized, the formation of orthopyroxene occurred. We believe that the most important is the possibility for the formation of Fe-silicates or oxides as a result of the carbide–sulfur–oxide interaction, and the fact that mantle silicate or oxide will play a role of a container for FeO depending on the composition of the crystallization medium.

In the present study we show the results of the interaction of iron carbide with S-rich fluids and melts, which can be expected to occur

Table 3
Averaged compositions of silicates, formed via carbide-sulfur-oxide interaction at 6.3 GPa and in the range of 900–1600 °C.

Run N	T, °C	Capsule material	Phase	N_A	Mass concentrations, wt.%				n(O)	Cations per formula unit				Fe#
					SiO_2	FeO	MgO	Total		Si	Fe	Mg	Sum	
O-1623	900	Gr	OPx_1	12	54.8 (2)	19.0 (4)	25.7 (3)	99.5 (1)	6	2.00 (1)	0.58 (1)	1.41 (1)	4.00 (1)	29.2
			OPx_2	10	45.7 (3)	54.0 (2)	–	99.9 (3)	6	2.00 (1)	1.99 (1)	–	4.00 (1)	100.0
O-1603	1000	Gr	OPx	12	57.4 (9)	8.9 (2)	33.2 (9)	99.5 (5)	6	2.00 (2)	0.26 (0)	1.74 (3)	4.00 (2)	13.0
O-1620	1100	Gr	OPx	10	56.4 (8)	7.9 (12)	35.3 (8)	99.5 (4)	6	1.96 (1)	0.23 (4)	1.84 (3)	4.03 (1)	11.1
O-1619	1200	Gr	OPx	11	58.1 (7)	6.3 (13)	35.2 (8)	99.7 (3)	6	2.00 (1)	0.18 (4)	1.82 (3)	4.00 (1)	9.1
O-1599	1300	Gr	OPx	9	59.1 (6)	4.6 (13)	35.9 (11)	99.5 (2)	6	2.02 (1)	0.13 (4)	1.84 (5)	3.98 (1)	6.7
O-1618	1400	Gr	OPx	12	58.4 (4)	4.3 (15)	37.1 (8)	99.9 (4)	6	1.99 (0)	0.12 (4)	1.89 (3)	4.01 (0)	6.2
O-1596	1500	Gr	OPx	12	59.4 (2)	3.8 (4)	36.3 (3)	99.5 (1)	6	2.02 (1)	0.11 (1)	1.85 (1)	3.98 (1)	5.5
O-1607	1500	Gr	OPx	8	58.9 (3)	3.6 (3)	36.5 (6)	99.0 (3)	6	2.01 (1)	0.10 (1)	1.87 (1)	3.99 (0)	5.2
			Ol	9	41.7(4)	3.6(6)	54.5(5)	99.8(4)	4	0.99(1)	0.07(2)	1.95(2)	3.01(0)	3.4
O-1602	1600	Gr	OPx	11	58.6 (2)	3.1 (4)	38.0 (3)	99.7 (1)	6	1.99 (1)	0.09 (1)	1.94 (1)	4.01 (1)	4.3
O-1593	1100	Ta	OPx	8	59.5 (5)	2.4 (19)	37.7 (19)	99.6 (3)	6	2.01 (1)	0.07 (6)	1.90 (8)	3.99 (1)	3.5
			Ol	10	42.0 (3)	2.1 (9)	55.5 (9)	99.5 (2)	4	0.99 (1)	0.04 (2)	1.97 (2)	3.01 (0)	2.0
O-1592	1200	Ta	OPx	9	59.2 (3)	1.0 (2)	39.3 (3)	99.6 (4)	6	1.99 (1)	0.03 (1)	1.98 (1)	4.01 (1)	1.4
			Ol	9	42.1 (3)	1.1 (2)	56.8 (4)	99.9 (5)	4	0.99 (1)	0.02 (1)	2.00 (2)	3.01 (1)	1.0
O-1588	1400	MgO	OPx	10	59.4 (2)	0.6 (1)	39.5 (2)	99.4 (3)	6	2.00 (0)	0.02 (0)	1.99 (1)	4.00 (0)	0.8
			Ol	10	42.3 (1)	0.3 (1)	57.2 (2)	99.8 (6)	4	0.99 (1)	0.01 (1)	2.01 (1)	3.01 (1)	0.3

Notes: OPx – orthopyroxene; Ol – olivine; Gr – graphite; Ta – talc ceramics; N_A - number of electron probe analyses used to obtain the average compositions. The values in parentheses are one sigma errors of the means based on replicate electron microprobe analyses reported as least units cited; 4.3 (15) should be read as 4.3 ± 1.5 wt.%; n(O) - number of oxygen atoms.

in micro-volumes in various environments of deep reduced mantle. Interaction of iron carbide-bearing rocks with S-rich fluids and sulfide melts, which both are believed to be reducing mantle metasomatic agents, has a series of consequences. When these metasomatic agents occur, iron carbide is unstable, and, depending on temperature, it can be partially or totally consumed to form cohenite + pyrrhotite + graphite assemblage (≤1100 °C) or to produce graphite or diamond, coexisting with Fe-S and Fe-S-C melts (≥1200 °C). Experimentally substantiated mechanism of graphite and diamond crystallization in assemblage with mantle sulfides and sulfide melts, via extraction of carbon from iron carbide through interaction with S-rich reduced melts and fluids, can be considered as one of the reasons for the formation of sulfide or sulfide + graphite inclusions in diamonds (Bulanova, 1995; Efimova et al., 1983; Sharp, 1966). Polymineral central inclusions in diamonds, consisting of carbide + graphite and sulfide + graphite (Bulanova, 1995) may be an indicator of the occurrence of such processes in nature.

5. Conclusions

Summarizing the results of the present study, the following conclusions can be drawn:

1) During carbide–sulfide, carbide–sulfur and carbide–sulfur–oxide interactions at a pressure of 6.3 GPa, graphite and/or diamond crystallization via extraction of carbon from carbide occurs in the temperature range of 900–1600 °C. Iron carbide can potentially act as a source of elemental carbon for diamond and graphite formation under reduced lithospheric mantle conditions. When S-bearing reduced fluid or sulfide melt is present, cohenite is unstable at temperatures higher than 1100 °C under lithospheric mantle pressures.
2) As a result of the interaction of cohenite with S-rich reduced fluid in the range of 900–1100 °C, graphite is formed associated to pyrrhotite and cohenite. At higher temperatures interaction of carbide with sulfide melt results in complete consumption of the cohenite and generation of a metal-sulfide melt with dissolved carbon ($Fe_{53\text{-}68}S_{30\text{-}40}C_{1\text{-}6.5}$, at.%), acting as a graphite (1200–1600 °C) and diamond (1300–1600 °C) crystallization medium.
3) During carbide-oxide reactions under the presence of S-rich reduced fluid, crystallization of graphite (900–1600 °C) or diamond growth on seeds (1400–1600 °C) is accompanied by the formation of a ferrous orthopyroxene and pyrrhotite (or sulfide melt).
4) A main mechanism of graphite and diamond crystallization via cohenite–sulfur and cohenite–sulfide interaction is supposed to involve extraction of carbon and iron from carbide into S-rich fluid or sulfide melt, formation of metal-sulfide melt with dissolved carbon and crystallization of graphite and diamond growth in this carbon-saturated melt.

Acknowledgements

This work was supported by the Russian Foundation for Basic Research (project No. 16-35-60024) and by a State Assignment (project no. 0330-2016-0007). The authors thank the editor Marco Scambelluri, the reviewer Fabrizio Nestola and an anonymous reviewer for their helpful and constructive reviews. The authors thank A. Moskalev and M. Jolivet for their assistance in the work preparation, A. Sokol and A. Khokhryakov for useful suggestions throughout the study, S. Ovchinnikov for his assistance in implementation of the Mössbauer spectroscopy measurements.

Appendix A. Supplementary data

Supplementary data to this article can be found online at http://dx.doi.org/10.1016/j.lithos.2017.06.010.

References

Alard, O., Lorand, J.-P., Reisberg, L., Bodinier, J.-L., Dautria, J.-M., O'Reilly, S., 2011. Volatile-rich metasomatism in Montferrier xenoliths (Southern France): implications for the abundances of chalcophile and highly siderophile elements in the subcontinental mantle. Journal of Petrology 52:2009–2045. http://dx.doi.org/10.1093/petrology/egr038.

Ballhaus, C., 1995. Is the upper mantle metal-saturated? Earth and Planetary Science Letters 132:75–86. http://dx.doi.org/10.1016/0012-821X(95)00047-G.

Ballhaus, C., Frost, B.R., 1994. The generation of oxidized CO_2-bearing basaltic melts from reduced CH_4-bearing upper mantle sources. Geochimica et Cosmochimica Acta 58: 4931–4940. http://dx.doi.org/10.1016/0016-7037(94)90222-4.

Bataleva, Yu.V., Palyanov, Yu.N., Borzdov, Yu.M., Bayukov, O.A., Sobolev, N.V., 2015. Interaction of iron carbide and sulfur under P-T conditions of the lithospheric mantle. Doklady Earth Sciences 463:707–711. http://dx.doi.org/10.1134/S1028334X15070077.

Bataleva, Yu.V., Palyanov, Yu.N., Borzdov, Yu.M., Bayukov, O.A., Sobolev, N.V., 2016a. Conditions for diamond and graphite formation from iron carbide at the P-T parameters of lithospheric mantle. Russian Geology and Geophysics 57:176–189. http://dx.doi.org/10.1016/j.rgg.2016.01.012.

Bataleva, Y.V., Palyanov, Y.N., Borzdov, Y.M., Sobolev, N.V., 2016b. Sulfidation of silicate mantle by reduced S-bearing metasomatic fluids and melts. Geology 44 (4): 271–274. http://dx.doi.org/10.1130/G37477.1.

Boehler, R., 1992. Melting of the Fe-FeO and the Fe-FeS systems at high pressure – constraints on core temperatures. Earth and Planetary Science Letters 111:217–227. http://dx.doi.org/10.1016/0012-821X(92)90180-4.

Brazhkin, V.V., Popova, S.V., Voloshin, R.N., 1999. Pressure-temperature phase diagram of molten elements: selenium, sulfur and iodine. Physica B: Condensed Matter 265: 64–71. http://dx.doi.org/10.1016/S0921-4526(98)01318-0.

Brett, R., 1967. Cohenite: its occurrence and a proposed origin. Geochimica et Cosmochimica Acta 31:143–159. http://dx.doi.org/10.1016/S0016-7037(67)80042-5.

Bulanova, G.P., 1995. Formation of diamond. Journal of Geochemical Exploration 53, 1–23.

Dasgupta, R., 2013. Ingassing, storage, and outgassing of terrestrial carbon through geologic time. Reviews in Mineralogy and Geochemistry 75:183–229. http://dx.doi.org/10.2138/rmg.2013.75.7.

Dasgupta, R., Hirschmann, M.M., 2010. The deep carbon cycle and melting in Earth's interior. Earth and Planetary Science Letters 298:1–13. http://dx.doi.org/10.1016/j.epsl.2010.06.039.

Dasgupta, R., Buono, A., Whelan, G., Walker, D., 2009. High-pressure melting relations in Fe–C–S systems: implications for formation, evolution, and structure of metallic cores in planetary bodies. Geochimica et Cosmochimica Acta 73: 6678–6691. http://dx.doi.org/10.1016/j.gca.2009.08.001.

Delpech, G., Lorand, J.P., Grégoire, M., Cottin, J.-Y., O'Reilly, S.Y., 2012. In-situ geochemistry of sulfides in highly metasomatized mantle xenoliths from Kerguelen, southern Indian Ocean. Lithos 154:296–314. http://dx.doi.org/10.1016/j.lithos.2012.07.018.

Deng, L., Fei, Y., Liu, X., Gong, Z., Shahar, A., 2013. Effect of carbon, sulfur and silicon on iron melting at high pressure: implications for composition and evolution of the planetary terrestrial cores. Geochimica et Cosmochimica Acta 114:220–233. http://dx.doi.org/10.1016/j.gca.2013.01.023.

Efimova, E.S., Sobolev, N.V., Pospelova, L.N., 1983. Sulphide inclusions in diamonds and features of their parageneses. Zapiski Vsesoyuznogo Mineralogicheskogo Obshchestva 112 (3), 300–310 (in Russian).

Eggler, D.H., Lorand, J.P., 1993. Mantle sulfide geobarometry. Geochimica et Cosmochimica Acta 57:2213–2222. http://dx.doi.org/10.1016/0016-7037(93)90563-C.

Evans, K.A., 2012. The redox budget of subduction zones. Earth-Science Reviews 113: 11–32. http://dx.doi.org/10.1016/j.earscirev.2012.03.003.

Evans, K.A., Powell, R., 2015. The effect of subduction on the sulphur, carbon and redox budget of lithospheric mantle. Journal of Metamorphic Geology 33:649–670. http://dx.doi.org/10.1111/jmg.12140.

Frost, D.J., McCammon, C.A., 2008. The redox state of Earth's mantle. Annual Review of Earth and Planetary Sciences 36:389–420. http://dx.doi.org/10.1146/annurev.earth.36.031207.124322.

Frost, D.J., Liebske, C., Langenhorst, F., McCammon, C.A., 2004. Experimental evidence for the existence of iron-rich metal in the Earth's lower mantle. Nature 428:409–412. http://dx.doi.org/10.1038/nature02413.

Gao, L., Chen, B., Zhao, J., Alp, E.E., Sturhahn, W., Li, J., 2011. Effect of temperature on sound velocities of compressed Fe_3C, a candidate component of the Earth's inner core. Earth and Planetary Science Letters 309:213–220. http://dx.doi.org/10.1016/j.epsl.2011.06.037.

Griffin, W.L., Graham, S., O'Reilly, S.Y., Pearson, N.J., 2004. Lithosphere evolution beneath the Kaapvaal Craton: Re–Os systematics of sulfides in mantle-derived peridotites. Chemical Geology 208:89–118. http://dx.doi.org/10.1016/j.chemgeo.2004.04.007.

Haggerty, S.E., 1986. Diamond genesis in a multiply constrained model. Nature 320: 34–48. http://dx.doi.org/10.1038/320034a0.

Jacob, D.E., Kronz, A., Viljoen, K.S., 2004. Cohenite, native iron and troilite inclusions in garnets from polycrystalline diamond aggregates. Contributions to Mineralogy and Petrology 146 (5):566–576. http://dx.doi.org/10.1007/s00410-003-0518-2.

Kaminsky, F.V., Wirth, R., 2011. Iron carbide inclusions in lower-mantle diamond from Juina, Brazil. Canadian Mineralogist 49:555–572. http://dx.doi.org/10.3749/canmin.49.2.555.

Lin, J.F., Fei, Y., Sturhahn, W., Zhao, J., Mao, H.K., Hemley, R.J., 2004. Magnetic transition and sound velocities of Fe_3S at high pressure: implications for Earth and planetary cores. Earth and Planetary Science Letters 226 (1–2):33–40. http://dx.doi.org/10.1016/j.epsl.2004.07.018.

Löfquist, H., Benedicks, S., 1941. Det store Nordenskjöldska Jarnblocket fran Ovifak; Mikrostruktur och Bildnigssät. Kungliga Svenska Vetenskapsakademiens Handlingar 19 (3) (96 pp.).

Lord, O.T., Walter, M.J., Dasgupta, R., Walker, D., Clark, S.M., 2009. Melting in the Fe–C system to 70 GPa. Earth and Planetary Science Letters 284:157–167. http://dx.doi.org/10.1016/j.epsl.2009.04.017.

Luth, R.W., 1999. Carbon and carbonates in mantle, in: Fei, Y., Bertka, M.C., Mysen, B.O. (eds.), Mantle Petrology: Field Observation and High Pressure Experimentation: A Tribute to Francis R. (Joe) Boyd. The Geochemical Society, Special Publication, No. 6, pp. 297-316.

Marty, B., 2012. The origins and concentrations of water, carbon, nitrogen and noble gases on Earth. Earth and Planetary Science Letters 313–314:56–66. http://dx.doi.org/10.1016/j.epsl.2011.10.040.

McCammon, C., 1997. Perovskite as a possible sink for ferric iron in the lower mantle. Nature 387:694–696. http://dx.doi.org/10.1038/42685.

Palyanov, Y.N., Borzdov, Y.M., Bataleva, Y.V., Sokol, A.G., Palyanova, G.A., Kupriyanov, I.N., 2007. Reducing role of sulfides and diamond formation in the Earth's mantle. Earth and Planetary Science Letters 260 (1–2):242–256. http://dx.doi.org/10.1016/j.epsl.2007.05.033.

Palyanov, Y.N., Borzdov, Y.M., Khokhryakov, A.F., Kupriyanov, I.N., Sokol, A.G., 2010. Effect of nitrogen impurity on diamond crystal growth processes. Crystal Growth and Design 10 (7):3169–3175. http://dx.doi.org/10.1021/cg100322p.

Palyanov, Y.N., Bataleva, Y.V., Sokol, A.G., Borzdov, Y.M., Kupriyanov, I.N., Reutsky, V.N., Sobolev, N.V., 2013. Mantle–slab interaction and redox mechanism of diamond formation. Proceedings of the National Academy of Sciences of the United States of America 110 (51):20408–20413. http://dx.doi.org/10.1073/pnas.1313340110.

Pal'yanov, Y.N., Sokol, A.G., Borzdov, Y.M., Khokhryakov, A.F., 2002. Fluid-bearing alkaline carbonate melts as the medium for the formation of diamonds in the Earth's mantle: an experimental study. Lithos 60 (3–4):145–159. http://dx.doi.org/10.1016/S0024-4937(01)00079-2.

Ramdohr, 1953. Neue Beobachtungen am Bühl-Eisen. Sitzungber Abhandlungen der Deutschen Akademie der Wissenschaften zu Berlin. Klasse für Mathematik und Allgemeine Naturwissenschaften 1952 (5), 9–24.

Ringwood, A.E., 1960. Cohenite as a pressure indicator in iron meteorites. Geochimica et Cosmochimica Acta 20:155–158. http://dx.doi.org/10.1016/0016-7037(60)90059-4.

Rohrbach, A., Schmidt, M.W., 2011. Redox freezing and melting in the Earth's deep mantle resulting from carbon – iron redox coupling. Nature 472:209–212. http://dx.doi.org/10.1038/nature09899.

Rohrbach, A., Ballhaus, C., Golla-Schindler, U., Ulmer, P., Kamenetsky, V.S., Kuzmin, D.V., 2007. Metal saturation in the upper mantle. Nature 449:456–458. http://dx.doi.org/10.1038/nature06183.

Rohrbach, A., Ghosh, S., Schmidt, M.W., Wijbrans, C.H., Klemme, S., 2014. The stability of Fe-Ni carbides in the Earth's mantle: evidence for a low Fe-Ni-C melt fraction in the deep mantle. Earth and Planetary Science Letters 388:211–221. http://dx.doi.org/10.1016/j.epsl.2013.12.007.

Schissel, D., Smail, R., 2001. Deep-mantle plumes and ore deposits. GSA Special Papers 352:291–322. http://dx.doi.org/10.1130/0-8137-2352-3.291.

Sharp, W.E., 1966. Pyrrhotite, a common inclusion in South African diamonds. Nature 21 (1):402–403. http://dx.doi.org/10.1038/211402b0.

Sharp, W.E., 1969. Melting curves of sphalerite, galena, and pyrrhotite and the decomposition curve of pyrite between 30 and 65 kilobars. Journal of Geophysical Research 74:1645–1652. http://dx.doi.org/10.1029/JB074i006p01645.

Smith, E.M., Kopylova, M.G., 2014. Implications of metallic iron for diamonds and nitrogen in the sublithospheric mantle. Canadian Journal of Earth Sciences 51 (5):510–516. http://dx.doi.org/10.1139/cjes-2013-0218.

Smith, E.M., Shirey, S.B., Nestola, F., Bullock, E.S., Wang, J., Richardson, S.H., Wang, W., 2016. Large gem diamonds from metallic liquid in Earth's deep mantle. Science 354 (6318):1403–1405. http://dx.doi.org/10.1126/science.aal1303.

Sobolev, N.V., 1974. Deep-seated Inclusions in Kimberlites and the Problem of the Composition of the Upper Mantle. Nauka, Novosibirsk (264 pp. (In Russian)).

Sobolev, N.V., Logvinova, A.M., Zedgenizov, D.A., Seryotkin, Y.V., Yefimova, E.S., Floss, C., Taylor, L.A., 2004. Mineral inclusions in microdiamonds and macrodiamonds from kimberlites of Yakutia: a comparative study. Lithos 77:225–242. http://dx.doi.org/10.1016/j.lithos.2004.04.001.

Sokol, A.G., Borzdov, Y.M., Palyanov, Y.N., Khokhryakov, A.F., 2015. High-temperature calibration of a multi-anvil high pressure apparatus. High Pressure Research 35 (2): 139–147. http://dx.doi.org/10.1080/08957959.2015.1017819.

Stagno, V., Tange, Y., Miyajima, N., McCammon, C.A., Irifune, T., Frost, D.J., 2011. The stability of magnesite in the transition zone and the lower mantle as function of oxygen fugacity. Geophysical Research Letters 38, L19309. http://dx.doi.org/10.1029/2011GL049560 (5 pp.).

Torsvik, T.K., Burke, K., Steinberger, B., Webb, S.J., Ashwal, L.D., 2010. Diamonds sampled by plumes from the core–mantle boundary. Nature 466:253–357. http://dx.doi.org/10.1038/nature09216.

Tsuno, K., Dasgupta, R., 2015. Fe-Ni-Cu-C-S phase relations at high pressures and temperatures – the role of sulfur in carbon storage and diamond stability at mid- to deep-upper mantle. Earth and Planetary Science Letters 412:132–142. http://dx.doi.org/10.1016/j.epsl.2014.12.018.

Wood, B.J., 1993. Carbon in the core. Earth and Planetary Science Letters 117:593–607. http://dx.doi.org/10.2138/rmg.2013.75.8.

Wood, B.J., Kiseeva, E.S., Mirolo, F.J., 2014. Accretion and core formation: the effects of sulfur on metal–silicate partition coefficients. Geochimica et Cosmochimica Acta 145:248–267. http://dx.doi.org/10.1016/j.gca.2014.09.002.

Woodland, A.B., Koch, M., 2003. Variation in oxygen fugacity with depth in the upper mantle beneath the Kaapvaal craton, Southern Africa. Earth and Planetary Science Letters 214:295–310. http://dx.doi.org/10.1016/S0012-821X(03)00379-0.

Zhang, Z., Hirschmann, M.M., 2015. Experimental constraints on mantle sulfide melting up to 8 GPa. American Mineralogist 101:181–192. http://dx.doi.org/10.2138/am-2016-5308.

Zhang, Z., Lentsch, N., Hirschmann, M.M., 2015. Carbon-saturated monosulfide melting in the shallow mantle: solubility and effect on solidus. Contributions to Mineralogy and Petrology 170:47. http://dx.doi.org/10.1007/s00410-015-1202-z.